INTERNATIONAL JOURNAL FOR NUMERICAL METHODS IN FLUIDS
Int. J. Numer. Meth. Fluids 2006; **51**:1255–1276
Published online 4 January 2006 in Wiley InterScience (www.interscience.wiley.com). DOI: 10.1002/fld.1150

Structured mesh generation with smoothness controls

Yaoxin Zhang[*,†,‡], Yafei Jia[§,¶] and Sam S. Y. Wang[‖,**]

National Center for Computational Hydroscience and Engineering, The University of Mississippi, P.O. Box 1500, Oxford, MS 38677, U.S.A.

SUMMARY

In geometrically complex domains, the Ryskin and Leal (RL) orthogonal mesh generation system may cause mesh distortion and overlapping problems when using the 'weak constraint' method with specified boundary point distribution for all boundaries. To resolve these problems, an improved RL system with automatic smoothness control is proposed. In this improved RL system, the automatic smoothness control mechanism is based on five types of smoothness conditions and includes the self-adjustment mechanism and the auto-evaluation mechanism for an empirical parameter. The proposed system is illustrated using several test examples. Several applications to natural domains are also demonstrated. It is shown that the improved RL system is capable of resolving the above problems at little cost of orthogonality. Copyright © 2006 John Wiley & Sons, Ltd.

KEY WORDS: mesh generation; smoothness control; self-adjustment mechanism; auto-evaluation mechanism

1. INTRODUCTION

Mesh generation is the art of mapping between the physical coordinates and the computational coordinates. Extensive researches (i.e. References [1–17]) in this area have been made. For a detailed review of researches and development in the 1990s, please refer to Reference [16].

It is well accepted that the mesh quality has significant influences on the solutions of the partial differential equations (PDE) regardless of the numerical method. According to the

[*]Correspondence to: Yaoxin Zhang, National Center for Computational Hydroscience and Engineering, The University of Mississippi, P.O. Box 1500, Oxford, MS 38677, U.S.A.
[†]E-mail: yzhang@ncche.olemiss.edu
[‡]Post-doctoral Research Associate.
[§]Research Associate Professor.
[¶]Assistant Director for Basic Research.
[‖]F.A.P. Barnard Distinguished Professor.
[**]Director.

Contract/grant sponsor: USDA Agriculture Research Service; contract/grant number: 58-6408-2-0062
Contract/grant sponsor: The University of Mississippi

Received 9 August 2005
Revised 7 November 2005
Accepted 7 November 2005

analysis of the truncation errors by Thompson *et al*. [15], generally the influences of the computational mesh on the solutions of PDE lie in two aspects: errors from the non-orthogonality and the non-smoothness. Thus, the orthogonality and the smoothness are considered as standard academic criterions to characterize the mesh quality. The goal of the quality mesh generation should emphasize on both the orthgonality and the smoothness. However, purely orthogonal and smooth meshes only exist in specific domains with simple geometries. For geometrically complex domains, they usually cannot be obtained simultaneously. Compromises must be made between them.

Since the late 1970s, orthogonal mesh generation has been the objective of many researchers [1, 2, 4–12]. The TTM system (a Poisson equation system with control functions) developed by Thompson *et al*. [14] and the Ryskin and Leal (RL) system (a Laplace equation system) proposed by Ryskin and Leal [11] are the most robust and widely used elliptic mesh generation systems. Another famous elliptic mesh generation system is the conformal mapping system, which is well known for orthogonal mapping with the equal scale factors in all directions. The TTM system is capable of producing orthogonal meshes or meshes with grid spacing controls according to the selections of the appropriate control functions, while the RL system, derived according to the analogue of the Laplace equation for the stream function and the velocity potential function, is aimed at orthogonal mapping without considering smoothness.

The effectiveness of the RL system for orthogonal mapping led to the wide use of this system [1, 2, 4, 5, 7, 9, 17]. However, because only the orthogonality is emphasized, when applying the RL system to geometrically complex domains using the 'weak constraint' method [11] in which the boundary point distribution is specified for all boundaries, problems such as mesh distortion and overlapping may occur, as demonstrated by Eça [5], Akcelik *et al.* [1] and Zhang *et al*. [17] in their researches. One way to resolve these problems is to introduce source terms (smoothness terms) into the RL system. Akcelik *et al*. [1] and Zhang *et al.* [17] used this method to alleviate the above problems. Another way is to directly control the distortion function f which is defined as a ratio of the scale factors in two different directions and plays an important role in orthogonal mapping. Usually the distortion function f is calculated by its definition. Allievi and Calisal [2], Eça [5] and Akcelik *et al*. [1] calculated f from its definition in the entire domain. Tamamidis and Assanis [12] used a Poisson equation to obtain a smooth variation of f in the entire domain. Duraiswami and Prosperetti [4] specified a class of admissible functions for f based on quasi-conformal mapping theory. Zhang *et al*. [17] introduced a contribution factor to confine the growth of f and hence avoid mesh distortion and overlapping problems.

In this paper, an improved RL system with automatic smoothness control is proposed, which is an extension of the work of Zhang *et al*. [17]. In their work, they introduced a contribution factor into the original RL system to control the effects of the distortion function f and successfully resolved mesh distortion and overlapping problems in geometrically complex domains. However, their proposed RL system was given only in discretized form and has an empirical parameter to tune for good results. In this study, the form of PDE is given for the modified RL system proposed in Reference [17], the physical meanings of this system is fully explored, and an automatic evaluation mechanism is established for that empirical parameter. Comparisons of the present method with other methods are made through several examples. Applications to natural estuaries are also demonstrated.

2. PREVIOUS STUDIES

One of the most widely used orthogonal generation systems is the RL system proposed by Ryskin and Leal [11].

2.1. RL system

From the mapping between the physical coordinates ($x^i(\equiv x, y), i = 1, 2$) and the computational coordinates ($\xi^i(\equiv \xi, \eta), i = 1, 2$), a metric tensor g_{ij} which represents the physical features of a mesh can be defined as follows:

$$g = \begin{Bmatrix} (x_\xi^2 + y_\xi^2) & (x_\xi x_\eta + y_\xi y_\eta) \\ (x_\xi x_\eta + y_\xi y_\eta) & (x_\eta^2 + y_\eta^2) \end{Bmatrix} \tag{1}$$

where $x_\xi = \partial x/\partial \xi$ and so forth.

Accordingly, the distortion function f (also called aspect ratio) is defined as the ratio of the scale factors in ξ and η direction:

$$f = \frac{h_\eta}{h_\xi} = \left(\frac{x_\eta^2 + y_\eta^2}{x_\xi^2 + y_\xi^2} \right)^{1/2} \tag{2a}$$

$$h_\xi = g_{11}^{1/2}, \quad h_\eta = g_{22}^{1/2} \tag{2b}$$

Analogue to the Laplace equations for stream function and velocity potential function leads to the following PDE:

$$\frac{\partial}{\partial \xi}\left(f \frac{\partial x}{\partial \xi} \right) + \frac{\partial}{\partial \eta}\left(\frac{1}{f} \frac{\partial x}{\partial \eta} \right) = 0 \tag{3a}$$

$$\frac{\partial}{\partial \xi}\left(f \frac{\partial y}{\partial \xi} \right) + \frac{\partial}{\partial \eta}\left(\frac{1}{f} \frac{\partial y}{\partial \eta} \right) = 0 \tag{3b}$$

Equation (3) is the Laplace mesh generation system proposed by Ryskin and Leal [11]. Using the central difference scheme to discretize Equation (3) at one typical mesh node (i, j), one can obtain:

$$F_{i,j} x_{i,j} = f_{i+1/2,j} x_{i+1,j} + f_{i-1/2,j} x_{i-1,j} + \frac{1}{f_{i,j+1/2}} x_{i,j+1} + \frac{1}{f_{i,j-1/2}} x_{i,j-1} \tag{4a}$$

$$F_{i,j} y_{i,j} = f_{i+1/2,j} y_{i+1,j} + f_{i-1/2,j} y_{i-1,j} + \frac{1}{f_{i,j+1/2}} y_{i,j+1} + \frac{1}{f_{i,j-1/2}} y_{i,j-1} \tag{4b}$$

where $F_{i,j} = f_{i+1/2,j} + f_{i-1/2,j} + (1/f_{i,j+1/2}) + (1/f_{i,j-1/2})$.

2.2. Improved RL system

The original RL system emphasizes on the orthogonality but ignores the smoothness of the mesh. It may cause serious mesh distortions and overlapping in geometrically complex

domains. To remedy this, Akcelik *et al.* [1] introduced the inhomogeneous source terms into the RL system, which controls favourably the scale factors and hence the aspect ratio of the resulting grid. In 2004, Zhang *et al.* [17] proposed an improved RL system with contribution factors which confine the contributions of the neighbours of mesh node (i,j) to control the mesh smoothness. Compared to the method of Akcelik *et al.* [1], this improved RL system can resolve the mesh distortions and overlapping problems completely with little cost of orthogonality.

In Reference [17], the improved RL system was given in the discretized forms as follows:

$$F_{i,j}x_{i,j} = f_{i+1/2,j}c_{i+1,j}x_{i+1,j} + f_{i-1/2,j}c_{i-1,j}x_{i-1,j} + \frac{c_{i,j+1}}{f_{i,j+1/2}}x_{i,j+1} + \frac{c_{i,j-1}}{f_{i,j-1/2}}x_{i,j-1} \tag{5a}$$

$$F_{i,j}y_{i,j} = f_{i+1/2,j}c_{i+1,j}y_{i+1,j} + f_{i-1/2,j}c_{i-1,j}y_{i-1,j} + \frac{c_{i,j+1}}{f_{i,j+1/2}}y_{i,j+1} + \frac{c_{i,j-1}}{f_{i,j-1/2}}y_{i,j-1} \tag{5b}$$

where $F_{i,j} = f_{i+1/2,j}c_{i+1,j} + f_{i-1/2,j}c_{i-1,j} + (c_{i,j+1}/f_{i,j+1/2}) + (c_{i,j-1}/f_{i,j-1/2})$ and $c_{i,j}$ is the contribution factor of mesh node (i,j) defined as follows:

$$c_{i+1,j} = (d_{i+1,j})^{\alpha} = (\sqrt{(x_{i,j} - x_{i+1,j})^2 + (y_{i,j} - y_{i+1,j})^2})^{\alpha} \tag{6a}$$

$$c_{i-1,j} = (d_{i-1,j})^{\alpha} = (\sqrt{(x_{i,j} - x_{i-1,j})^2 + (y_{i,j} - y_{i-1,j})^2})^{\alpha} \tag{6b}$$

$$c_{i,j+1} = (d_{i,j+1})^{\alpha} = (\sqrt{(x_{i,j} - x_{i,j+1})^2 + (y_{i,j} - y_{i,j+1})^2})^{\alpha} \tag{6c}$$

$$c_{i,j-1} = (d_{i,j-1})^{\alpha} = (\sqrt{(x_{i,j} - x_{i,j-1})^2 + (y_{i,j} - y_{i,j-1})^2})^{\alpha} \tag{6d}$$

where $d_{i+1,j}$ is the distance between point (i,j) and point $(i+1,j)$ and the exponential parameter $\alpha \in [0,1]$ is a empirical parameter.

The contribution factor is evaluated by the distance of the mesh node (i,j) and its neighbours and it can confine the unbounded growth of the distortion function within a reasonable range to avoid the mesh overlapping. The empirical parameter α is an adjustable parameter used to control the strength of the contribution factors.

3. PRESENT STUDY

The improved RL system defined by Equation (5) is capable of producing meshes in geometrically complex domains without mesh distortion and overlapping problems if an appropriate value of the empirical parameter α is selected. Without an automatic evaluation mechanism, the manual evaluation process for this parameter would be tedious in order to obtain good results. In this paper, further researches have been conducted on the improved RL system proposed by Zhang *et al.* [17]. An automatic smoothness control method has been developed.

3.1. Elliptic equations

In Reference [17], only the discretized equations were given. Using the central difference scheme, the following relationships can be obtained:

$$c_{i+1,j} = (d_{i+1,j})^{\alpha} = [(h_{\xi})_{i+1/2,j}]^{\alpha} \tag{7a}$$

$$c_{i-1,j} = (d_{i-1,j})^{\alpha} = [(h_{\xi})_{i-1/2,j}]^{\alpha} \tag{7b}$$

$$c_{i,j+1} = (d_{i,j+1})^{\alpha} = [(h_{\eta})_{i,j+1/2}]^{\alpha} \tag{7c}$$

$$c_{i,j-1} = (d_{i,j-1})^{\alpha} = [(h_{\eta})_{i,j-1/2}]^{\alpha} \tag{7d}$$

Notice that the subscripts 'ξ' and 'η' in h_{ξ} and h_{η} do not denote the first-order derivatives (FOD) with respect to ξ and η. Substituting Equation (7) into Equation (5) and then rearranging it, the following PDE of the improved RL system can be obtained:

$$\frac{\partial}{\partial \xi}\left(h_{\xi}^{\alpha} \cdot f \frac{\partial x}{\partial \xi}\right) + \frac{\partial}{\partial \eta}\left(h_{\eta}^{\alpha} \cdot \frac{1}{f} \frac{\partial x}{\partial \eta}\right) = 0 \tag{8a}$$

$$\frac{\partial}{\partial \xi}\left(h_{\xi}^{\alpha} \cdot f \frac{\partial y}{\partial \xi}\right) + \frac{\partial}{\partial \eta}\left(h_{\eta}^{\alpha} \cdot \frac{1}{f} \frac{\partial y}{\partial \eta}\right) = 0 \tag{8b}$$

Another form of Equation (8) is used in order to understand the physical meanings of the improved RL system, i.e. as follows:

$$X_{\mathrm{O}} + X_{\mathrm{S}} = 0 \tag{9a}$$

$$Y_{\mathrm{O}} + Y_{\mathrm{S}} = 0 \tag{9b}$$

$$X_{\mathrm{O}} = \frac{\partial}{\partial \xi}\left(f \frac{\partial x}{\partial \xi}\right) + \frac{\partial}{\partial \eta}\left(\frac{1}{f} \frac{\partial x}{\partial \eta}\right) \tag{9c}$$

$$Y_{\mathrm{O}} = \frac{\partial}{\partial \xi}\left(f \frac{\partial y}{\partial \xi}\right) + \frac{\partial}{\partial \eta}\left(\frac{1}{f} \frac{\partial y}{\partial \eta}\right) \tag{9d}$$

$$X_{\mathrm{S}} = \alpha \frac{1}{h_{\xi}} \frac{\partial h_{\xi}}{\partial \xi} \cdot f x_{\xi} + \alpha \frac{f^{\alpha}}{h_{\eta}} \frac{\partial h_{\eta}}{\partial \eta} \cdot \frac{1}{f} x_{\eta} + (f^{\alpha} - 1) \frac{\partial}{\partial \eta}\left(\frac{1}{f} \frac{\partial x}{\partial \eta}\right) \tag{9e}$$

$$Y_{\mathrm{S}} = \alpha \frac{1}{h_{\xi}} \frac{\partial h_{\xi}}{\partial \xi} \cdot f y_{\xi} + \alpha \frac{f^{\alpha}}{h_{\eta}} \frac{\partial h_{\eta}}{\partial \eta} \cdot \frac{1}{f} y_{\eta} + (f^{\alpha} - 1) \frac{\partial}{\partial \eta}\left(\frac{1}{f} \frac{\partial y}{\partial \eta}\right) \tag{9f}$$

where the subscript 'O' denotes orthogonality and the subscript 'S' denotes smoothness.

Both Equations (8) and (9) represent the improved RL system. Equation (8) is in conservative form, while Equation (9) is a Poisson equation. As shown in Equations (9a) and (9b), the improved RL system consists of two parts, the orthogonality part (X_{O} and Y_{O}) driven by the left-hand side of the original RL system, and the smoothness part (X_{S} and Y_{S}) controlled

by the contribution factors. The smoothness part is divided into three components. In the right-hand side of Equations (9e) and (9f), the first term contains the FOD of the scale factor in ξ direction (h_ξ). Since the scale factor h_ξ also represents the arch length in ξ direction, the FOD of h_ξ can characterize the smoothness in ξ direction. Thus, the first term can be considered to avoid mesh overlapping in ξ direction. Similar to the first term, the second term is for the smoothness in η direction. As for the last term, according to its mathematical definition, the second-order derivative of x and y can characterize the distortion of the mesh line, so the last term is against mesh distortion.

Another form of the smoothness part (X_S and Y_S) can be easily derived.

$$X_S = \alpha \frac{1}{h_\xi \cdot f^\alpha} \frac{\partial h_\xi}{\partial \xi} \cdot f x_\xi + \alpha \frac{1}{h_\eta} \frac{\partial h_\eta}{\partial \eta} \cdot \frac{1}{f} x_\eta + \left(\frac{1}{f^\alpha} - 1\right) \frac{\partial}{\partial \xi}\left(f \frac{\partial x}{\partial \xi}\right) \tag{10a}$$

$$Y_S = \alpha \frac{1}{h_\xi \cdot f^\alpha} \frac{\partial h_\xi}{\partial \xi} \cdot f y_\xi + \alpha \frac{1}{h_\eta} \frac{\partial h_\eta}{\partial \eta} \cdot \frac{1}{f} y_\eta + \left(\frac{1}{f^\alpha} - 1\right) \frac{\partial}{\partial \xi}\left(f \frac{\partial y}{\partial \xi}\right) \tag{10b}$$

Notice that each component in smoothness part (X_S and Y_S) defined by Equations (9e) and (9f) are not equal to its counterpart defined by Equations (10a) and (10b), but both have the same physical meanings.

3.2. Self-adjustment mechanism

In Equation (9), obviously the empirical parameter α has influences on the smoothness part. To look deep into each component of the smoothness part, the effect of α will be excluded in the following discussions.

The effect of the first smoothness component is also determined by the FOD of the scale factor in ξ direction. The zero value of this FOD (called *smoothness condition in ξ direction*) can make this component disappear in Equation (9). The physical meaning of this smoothness condition can be interpreted in two different scopes. At one typical mesh node (i, j), it implies that the local scale factor is equal to the local averaged scale factor in ξ direction, as described in Equation (11).

$$\begin{aligned}
&\left(\frac{\partial h_\xi}{\partial \xi}\right)_{i,j} \approx (h_\xi)_{i+1/2,j} - (h_\xi)_{i-1/2,j} = 0 \\
&\Rightarrow (h_\xi)_{i+1/2,j} = (h_\xi)_{i-1/2,j} \\
&\Rightarrow [(x_{i,j} - x_{i+1,j})^2 + (y_{i,j} - y_{i+1,j})^2]^{1/2} = [(x_{i,j} - x_{i-1,j})^2 + (y_{i,j} - y_{i-1,j})^2]^{1/2} \\
&\Rightarrow x_{i,j} = \frac{x_{i-1,j} + x_{i+1,j}}{2}, \quad y_{i,j} = \frac{y_{i-1,j} + y_{i+1,j}}{2} \\
&\Rightarrow (h_\xi)_{i,j} = \frac{(h_\xi)_{i+1/2,j} + (h_\xi)_{i-1/2,j}}{2} = (\overline{h_\xi})_{i,j}
\end{aligned} \tag{11}$$

where $(\overline{h_\xi})_{i,j}$ is the local averaged scale factor.

If this smoothness condition is satisfied in the entire domain, that is, Equation (11) is satisfied for each mesh node, one can have:

$$(h_\xi)_{i,j} = (\overline{h_\xi})_i = \frac{1}{N_j - 2} \sum_{j=2}^{N_j - 1} (h_\xi)_{i,j} \tag{12}$$

where $(\overline{h_\xi})_i$ is the global averaged scale factor at $\xi = i$ line, and N_j is the total number of mesh lines in η direction.

Similarly, for the second smoothness component, the local satisfaction of the zero value of the FOD (called *smoothness condition in η direction*) implies the following equation:

$$\begin{aligned} \frac{\partial h_\eta}{\partial \eta} &\approx (h_\eta)_{i,j+1/2} - (h_\eta)_{i,j-1/2} = 0 \\ \Rightarrow (h_\eta)_{i,j} &= \frac{(h_\eta)_{i,j+1/2} + (h_\eta)_{i,j-1/2}}{2} = (\overline{h_\eta})_{i,j} \end{aligned} \tag{13}$$

where $(\overline{h_\eta})_{i,j}$ is the local averaged scale factor.

If this smoothness condition is globally satisfied, one can obtain:

$$(h_\eta)_{i,j} = (\overline{h_\eta})_j = \frac{1}{N_i - 2} \sum_{i=2}^{N_i - 1} (h_\eta)_{i,j} \tag{14}$$

where $(\overline{h_\eta})_j$ is the global averaged scale factor at $\eta = j$ line, and N_i is the total number of mesh lines in ξ direction.

Because Equations (12) and (14) are much stricter than their counterparts—Equations (11) and (13), Equations (11) and (13) are called *relative smoothness condition in ξ and η direction*, while Equations (12) and (14) are called *absolute smoothness condition in ξ and η directions*, respectively.

As for the last smoothness component in Equation (9), the distortion function f plays an important role. If $f = 1$, this component will vanish, which is equivalent to the *absolute smoothness condition*, because for one mesh node (i, j), this condition can be described by

$$f_{i,j} = 1 \Rightarrow (h_\xi)_{i,j} = (h_\eta)_{i,j} \tag{15}$$

For most cases, especially those with complex geometry, this absolute smoothness condition is too strict to be satisfied for the entire domain. Satisfaction of this condition for the whole domain also implies the smoothness conditions described by Equations (11)–(14), and accordingly, Equation (9) will turn to the following conformal mapping system.

$$\frac{\partial^2 x}{\partial \xi^2} + \frac{\partial^2 x}{\partial \eta^2} = 0 \tag{16a}$$

$$\frac{\partial^2 y}{\partial \xi^2} + \frac{\partial^2 y}{\partial \eta^2} = 0 \tag{16b}$$

As a summary, the FOD of the scale factor and the distortion function f can automatically adjust the effect of the smoothness part independent of the exponential parameter α

according to the local smoothness conditions. The smoother the mesh is, the smaller will be the effects of the smoothness part, and vice versa. Since the *absolute smoothness condition* defined by Equation (15) is much stronger than the *relative smoothness conditions* defined by Equations (11) and (13), the adjustment mechanism for the first two smoothness components according to the FOD of the scale factor is more effective than the one for the last smoothness component due to the distortion function f.

For one mesh node (i, j), the deviation from the local smoothness conditions defined by Equations (11)–(15) (DLS) can be measured by the following indicators:

$$(\mathrm{DLS})_{\xi}^{\mathrm{Local}}|_{i,j} = \frac{|(h_{\xi})_{i,j} - (\overline{h_{\xi}})_{i,j}|}{(\overline{h_{\xi}})_{i,j}} \tag{17a}$$

$$(\mathrm{DLS})_{\eta}^{\mathrm{Local}}|_{i,j} = \frac{|(h_{\eta})_{i,j} - (\overline{h_{\eta}})_{i,j}|}{(\overline{h_{\eta}})_{i,j}} \tag{17b}$$

$$(\mathrm{DLS})_{\xi}^{\mathrm{Global}}|_{i,j} = \frac{|(h_{\xi})_{i,j} - (\overline{h_{\xi}})_{i}|}{(\overline{h_{\xi}})_{i}} \tag{17c}$$

$$(\mathrm{DLS})_{\eta}^{\mathrm{Global}}|_{i,j} = \frac{|(h_{\eta})_{i,j} - (\overline{h_{\eta}})_{j}|}{(\overline{h_{\eta}})_{j}} \tag{17d}$$

$$(\mathrm{DLS})_{i,j} = \frac{|(h_{\xi})_{i,j} - (h_{\eta})_{i,j}|}{\max[(h_{\xi})_{i,j}, (h_{\eta})_{i,j}]} \tag{17e}$$

where the superscript '*Local*' denotes the use of the local averaged scale factors, and the superscript '*Global*' denotes the use of the global averaged scale factors.

In Equation (17), $(\mathrm{DLS})_{\xi}^{\mathrm{Local}}|_{i,j}$ and $(\mathrm{DLS})_{\eta}^{\mathrm{Local}}|_{i,j}$ (the deviations from the local *relative smoothness conditions*) are used to measure the local effects of the FOD of the scale factor in the first two smoothness components, respectively, while $(\mathrm{DLS})_{i,j}$ (the deviation from the local *absolute smoothness condition*) is used to measure the local effect of the distortion function f in the last smoothness component. As for $(\mathrm{DLS})_{\xi}^{\mathrm{Global}}|_{i,j}$ and $(\mathrm{DLS})_{\eta}^{\mathrm{Global}}|_{i,j}$, they are used to measure the deviations from the local *absolute smoothness conditions in ξ and η directions*, respectively.

Among the above five indicators, $(\mathrm{DLS})_{\xi}^{\mathrm{Local}}|_{i,j}$, $(\mathrm{DLS})_{\eta}^{\mathrm{Local}}|_{i,j}$ and $(\mathrm{DLS})_{i,j}$ measure the smoothness only in a local scope, while $(\mathrm{DLS})_{\xi}^{\mathrm{Global}}|_{i,j}$ and $(\mathrm{DLS})_{\eta}^{\mathrm{Global}}|_{i,j}$ consider the global smoothness along individual mesh lines. Each indicator can measure only one aspect of the local smoothness. Good indication (small value) of one indicator does not necessarily mean the good local smoothness. To characterize the local smoothness comprehensively, the following combination of these indicators can be used:

$$\lambda_1(\mathrm{DLS})_{\xi}^{\mathrm{Local}} + \lambda_2(\mathrm{DLS})_{\eta}^{\mathrm{Local}} + \lambda_3(\mathrm{DLS})_{\xi}^{\mathrm{Global}} + \lambda_4(\mathrm{DLS})_{\eta}^{\mathrm{Global}} + \lambda_5(\mathrm{DLS}) \tag{18a}$$

$$\sum_{1}^{5} \lambda_i = 1 \tag{18b}$$

In Equation (18), a combination for optimal local smoothness may exist depending on the importance of these indicators. In practice, it is difficult to evaluate the importance of these

indicators for mesh smoothness, because the optimal combination is case dependent. Further researches are needed in this regard. In the current study, the contribution from each of the five indicators is considered to be equally important. That is, an algebraic average of the above five indicators is used.

$$(\mathrm{ADS})_{i,j} = \left[\frac{(\mathrm{DLS})_{\xi}^{\mathrm{Local}} + (\mathrm{DLS})_{\eta}^{\mathrm{Local}} + (\mathrm{DLS})_{\xi}^{\mathrm{Global}} + (\mathrm{DLS})_{\eta}^{\mathrm{Global}} + (\mathrm{DLS})}{5} \right]_{i,j} \tag{19}$$

where ADS is the averaged deviations from local smoothness conditions.

3.3. Automatic evaluation mechanism

As discussed previously, the smoothness part has an independent self-adjustment mechanism due to the deviations from the local smoothness conditions. In Equation (5), the parameter α is an empirical adjustable parameter to control the strength of the contribution factors. The larger the α is, the more effective the contribution factors are, and the smoother will be the resulting mesh. To achieve the goal of automatic smoothness control using the improved RL system defined by Equation (8) or (9), an automatic evaluation mechanism must be also established for this empirical parameter α. Obviously, this auto-evaluation mechanism should be consistent with the self-adjustment mechanism of the smoothness part, which suggests that the evaluation of α be related to the local smoothness conditions. And, it should not be the repeating but the supplement of the self-adjustment mechanism.

Because the mesh distortion or mesh overlapping always occurs at places with large deviations from the local smoothness conditions, it appears that the empirical parameter α should have varied distributions in the whole domain. However, the spatial distribution of α implies that different equation systems would be solved at different mesh nodes. From a global point of view, this inconsistency may degenerate the overall quality of the mesh, or even influence the steadiness of the computation (it will be demonstrated by some examples). To avoid this inconsistency, a constant value of α instead should be used for each mesh node. And, to obtain a global smoothness improvement, this constant value should be controlled by the mesh node with the maximum deviations from the local smoothness conditions. For most mesh nodes with good smoothness, this constant value might be over-predicted and unnecessary. To reduce this influence it needs to comprehensively consider the local smoothness.

According to the above analysis, the maximum ADS is used to evaluate this empirical parameter. Then one can obtain:

$$\alpha = \max[\min(\mathrm{ADS}_{i,j}, 1)] \tag{20}$$

As demonstrated in Reference [17], α has big influence on mesh orthogonality and smoothness. The larger it is, the smoother and less orthogonal will be the mesh, and vice versa. Notice that Equation (20) implies that α is bounded within the range of $[0, 1]$. With the self-adjustment mechanism and the auto-evaluation mechanism for α, the automatic smoothness control on the mesh generation based on the improved RL system defined by Equation (8) or (9) is established. Although α cannot vary in space, it can vary with iterations, since an iteration process is usually used to solve Equation (8). During the iteration process, α is dynamically adjusted by Equation (20) at each step.

4. SOLUTION PROCESS

Since Equation (8) is nonlinear, an iteration process similar to that of Equation (20) is used to solve the linearized Equation (5). The maximum difference between the grid coordinates and the maximum relative difference of the distortion function f in consecutive steps are used as the convergence conditions. Satisfaction of either one will stop the computation.

$$\text{Error} = \max\left(\sqrt{(x_{i,j}^n - x_{i,j}^{n-1})^2 + (y_{i,j}^n - y_{i,j}^{n-1})^2}\right) < 10^{-6} \tag{21}$$

$$\text{Error} = \max\left(\frac{f^n - f^{n-1}}{f^n}\right) < 10^{-6} \tag{22}$$

where n is the iteration number.

The linear Equation (5) is solved iteratively using the following iterative algorithm:

(a) Define the boundaries of the domain and use an algebraic method to generate an initial mesh.
(b) Calculate the distortion function f from its definition Equation (2).
(c) Calculate the exponential parameter α using Equation (20).
(d) Calculate the contribution factors from Equation (6) using the most recent solutions.
(e) Solve Equation (5) with fixed f obtained from step (b), the fixed exponential parameter α from step (c) and the contribution factors from step (d).
(f) Update the mesh and check if the convergence condition is satisfied. If not, repeat steps from (b) to (f).

5. BOUNDARY CONDITIONS

The mesh generation based on the elliptic systems (Equations (3) and (8)) is an initial-boundary value problem, and the boundary conditions have significant influences on the resulting mesh. There are two kinds of boundary conditions widely used: the Dirichlet boundary condition and the Dirichlet–Neumann boundary condition. In the former boundary condition, the mesh nodes along the boundaries are fixed, while the latter allows the mesh nodes to slide along the boundaries (Dirichlet) to satisfy the Neumann condition, and therefore it is also called sliding boundary conditions.

The Dirichlet boundary condition is rigid and sometimes may cause the mesh distortion and mesh overlapping problems in geometrically complex domains. As demonstrated in References [1, 4, 17], in some complex domains these problems can be resolved by applying the sliding boundary conditions to the appropriate boundaries. In the present study, in order to purely test the effect of the improved RL system with automatic smoothness control, only the Dirichlet boundary conditions are used for all the boundaries.

6. EVALUATION OF MESH QUALITY

Brackbill and Saltzman [3] used three indices, orthogonality, smoothness and adaptivity, to evaluate the mesh quality. The orthogonality and the smoothness are standard academic criterions for mesh quality evaluation and they are usually measured by the following

indicators, maximum deviation orthogonality (MDO), averaged deviation from orthogonality (ADO), maximum grid aspect ratio (MAR), and averaged grid aspect ratio (AAR). As for the adaptivity, it measures the mesh density distribution according to the physics of a particular problem and sometimes it is more preferred. In the current study, only the standard academic criterions, the orthogonality and the smoothness, are used to evaluate the mesh quality.

The MDO and ADO, which are used to evaluate the orthogonality of a mesh, are defined as

$$\mathrm{MDO} = \max |\theta_{i,j} - 90| \tag{23a}$$

$$\mathrm{ADO} = \frac{1}{(N_i - 2)} \frac{1}{(N_j - 2)} \sum_{2}^{N_i - 1} \sum_{2}^{N_j - 1} |\theta_{i,j} - 90| \tag{23b}$$

where N_i and N_j are the maximum number of mesh lines in ξ and η directions, respectively, and θ is defined as

$$\theta_{i,j} = \arccos\left(\frac{g_{12}}{h_\xi h_\eta}\right)_{i,j} \tag{24}$$

The MAR and AAR, which are used to evaluate the smoothness of a mesh, are defined as

$$\mathrm{MAR} = \max\left[\max\left(f_{i,j}, \frac{1}{f_{i,j}}\right)\right] \tag{25a}$$

$$\mathrm{AAR} = \frac{1}{(N_i - 2)} \frac{1}{(N_j - 2)} \sum_{2}^{N_i - 1} \sum_{2}^{N_j - 1} \max\left(f_{i,j}, \frac{1}{f_{i,j}}\right) \tag{25b}$$

7. EXAMPLES

The proposed improved RL system defined by Equation (8) is compared with the original RL system defined by Equation (3), and the conformal mapping system defined by Equation (16) through several examples commonly used in the literatures [8–13]. The constant α in the whole domain (Equation (20)) is also compared with the spatially varied α which is evaluated by the following equation:

$$\alpha_{i,j} = \min(\mathrm{ADS}_{i,j}, 1) \tag{26}$$

In the following examples except for domain E, initial meshes with uniform nodal distribution along the four boundaries, namely, top boundary, bottom boundary, left boundary, and right boundary, were generated by the algebraic method. The Dirichlet boundary conditions are applied in all boundaries.

7.1. Symmetric domains

The symmetric domains A and B are selected to test the proposed method:

(1) Domain A (with concave boundary) is bounded by $x = 0$, $x = 1$, $y = 0$, and $y = 0.75 + 0.25\sin(\pi(0.5 + 2x))$.
(2) Domain B is a unit square with one half-circle on each side.

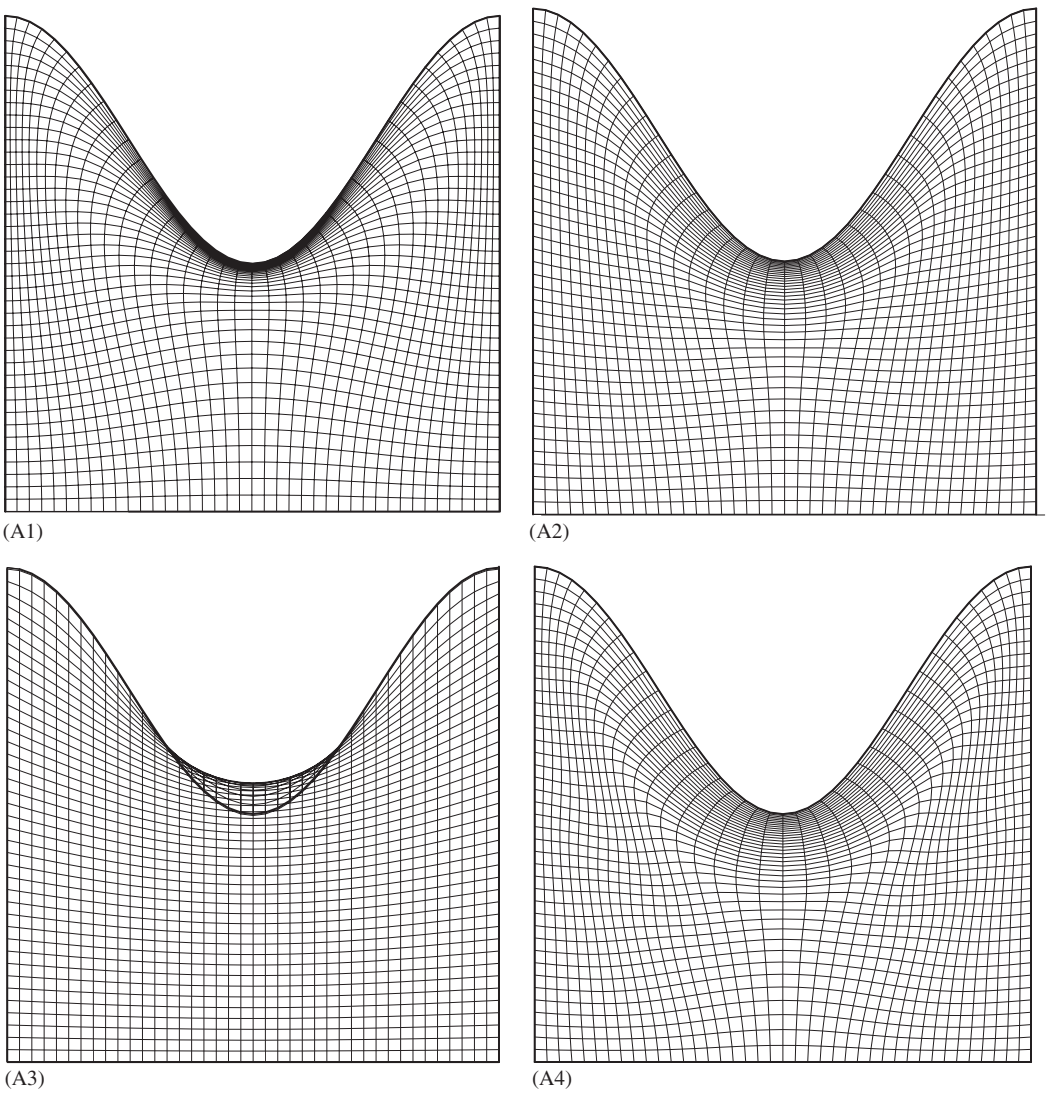

Figure 1. Meshes in domain A: (A1) RL; (A2) improved RL with constant α in the whole domain; (A3) conformal mapping; and (A4) improved RL with spatially varied α.

Meshes in domains A and B are plotted in Figures 1 and 2, respectively. The quality of meshes is summarized in Table I. The original RL system caused the mesh lines to be squeezed to the concaved top boundary in domain A, and to the centre of domain B. It generated the best orthogonal meshes with the worst smoothness. The improved RL system improved the mesh smoothness significantly with little cost of orthogonality. In domain A, slight mesh distortion occurred when using the spatially varied α. Using the constant α in the

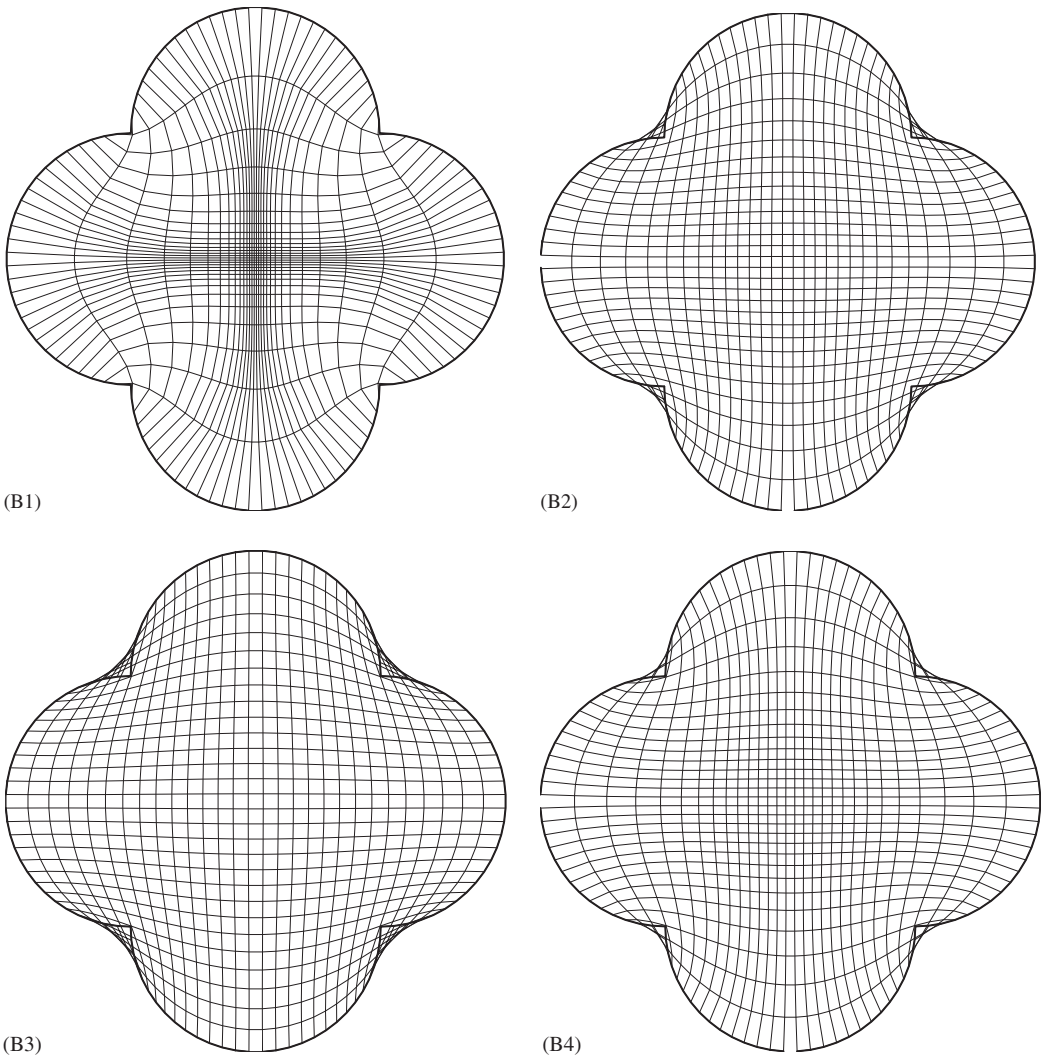

Figure 2. Meshes in domain B: (B1) RL; (B2) improved RL with constant α in the whole domain; (B3) conformal mapping; and (B4) improved RL with spatially varied α.

whole domain produced globally smoother meshes. The conformal mapping system generated folded meshes at the concave boundary. In domain B, because the improved RL system cannot handle the four corners well in domain B, the mesh lines moved outside of domain at the four corners. The same problem existed when using the conformal mapping system. One way to resolve these four corners is to apply the sliding boundary conditions to the four circular boundaries or specify the non-uniform nodal distributions along boundaries, as used by Duraiswami and Prosperetti [4].

Table I. Evaluation of meshes in domains A and B.

Domain	Case	Size	ADO	MDO	AAR	MAR	Final α
A	A1	41×41	0.07	0.62	4.86	33.9	—
	A2	41×41	2.29	5.03	2.49	10.9	0.403
	A3	41×41	3.18	11.62	2.98	411.3	—
	A4	41×41	1.68	4.82	2.64	9.26	—
B	B1	30×30	0.07	4.28	4.22	13.0	—
	B2	30×30	2.64	14.5	1.56	2.76	0.3
	B3	30×30	4.63	14.6	1.19	1.61	—
	B4	30×30	2.21	14.3	1.74	3.11	—

7.2. *Asymmetric domains*

Two asymmetric domains are used to further test the proposed methods.

(1) Domain C is bounded by $x = 0$, $y = 0$, $y = 1$, and $x = \frac{1}{2} + \frac{1}{6}\cos(\pi y)$.
(2) Domain D is bounded by two-half circles and x-axis. The radius of the small circle is one-third of that of the big one.

Figures 3 and 4 display the resulting meshes and Table II lists the evaluation report of mesh quality. Using the original RL system, serious mesh distortions and overlapping occurred within both domains. The improved RL with constant α in the whole domain successfully removed the mesh distortions and overlapping with the orthogonality suppressed a little, while the improved RL with the spatially varied α failed to generate sufficiently smooth meshes without distortion and overlapping. Similar to domain A, the conformal mapping system also failed to generate acceptable meshes for domain D.

The spatially varied α implies that different equations are solved at different mesh nodes. As demonstrated in domains A, C and D, this inconsistency may degenerate the overall mesh quality. Therefore, the constant α in the whole domain should be used in the improved RL system.

7.3. *Domain without distortion and overlapping problems*

A symmetric domain E is selected to further compare the original RL and the improved RL with constant α in the whole domain. This domain is bounded by $x = -2$, $x = 2$, $y = 0$ and $y = 2/[\exp(x) + \exp(-x)]$. The non-uniform and symmetric nodal distribution is applied along the top curved boundary.

The resulting meshes and their evaluations are displayed in Figure 5 and Table III. As can be seen, these two methods have very similar performances, and both succeeded in generating meshes without distortion and overlapping problems. The original RL is slightly better in orthogonality, while the improved RL with constant α in the whole domain is a little better in smoothness.

7.4. *Convergence analysis*

Figure 6 shows the convergence processes for domains A–D when using the improved RL system with constant α in the whole domain. In Figure 6, the error is defined by Equation (21).

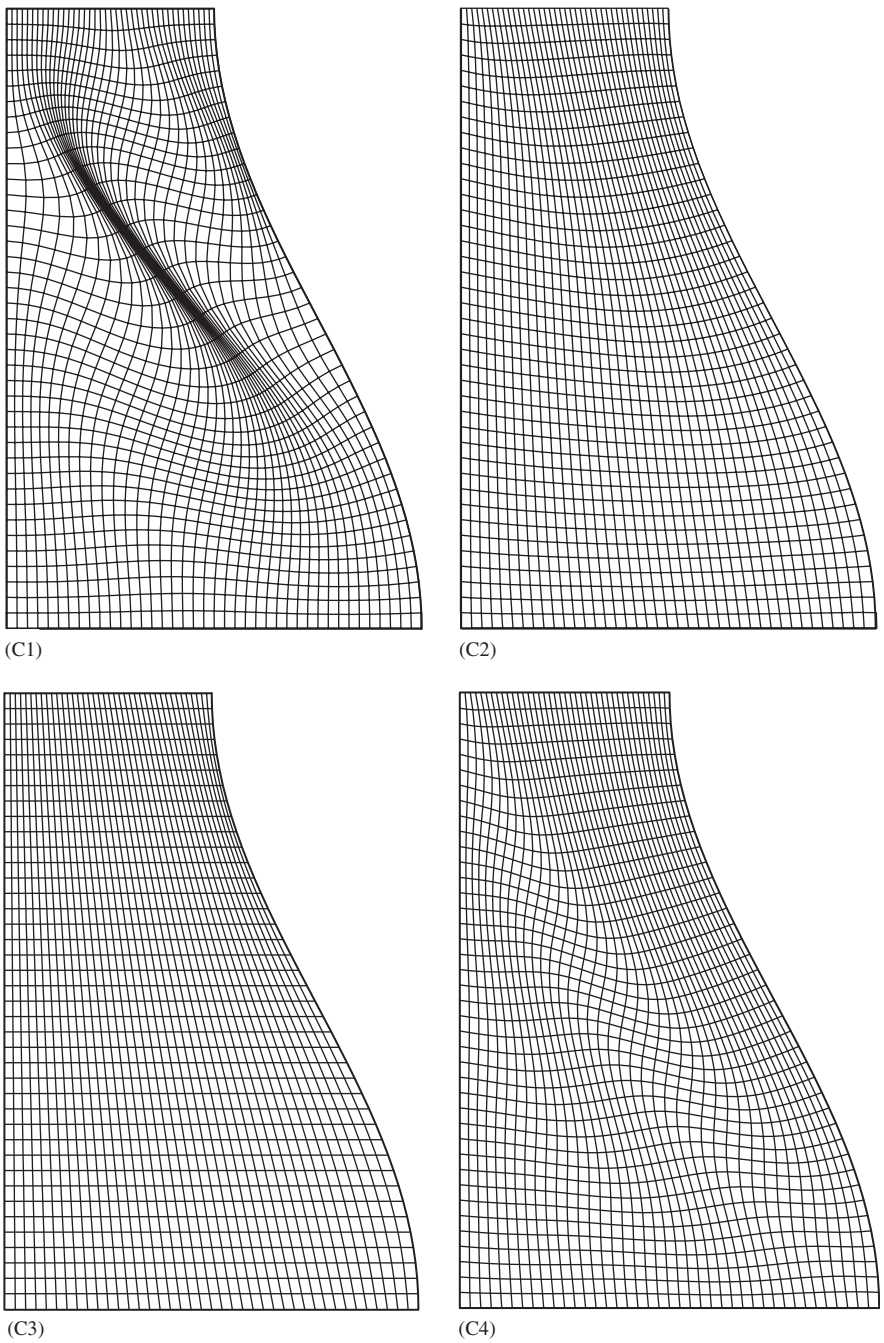

Figure 3. Meshes in domain C: (C1) RL; (C2) improved RL with constant α in the whole domain; (C3) conformal mapping; and (C4) improved RL with spatially varied α.

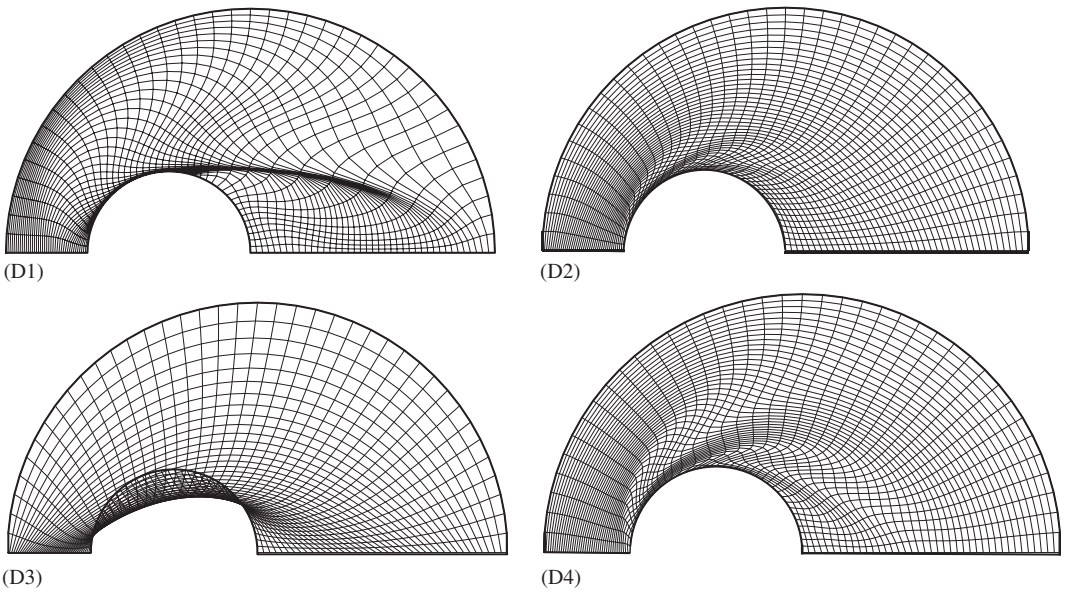

Figure 4. Meshes in domain D: (D1) RL; (D2) improved RL with constant α in the whole domain; (D3) conformal mapping; and (D4) improved RL with spatially varied α.

Table II. Evaluation of meshes in domains C and D.

Domain	Case	Size	ADO	MDO	AAR	MAR	Final α
C	C1	41×41	0.37	1.11	3.98	46.1	—
	C2	41×41	2.02	3.37	2.24	3.74	0.212
	C3	41×41	2.33	6.32	2.17	5.11	—
	C4	41×41	1.71	3.41	2.30	3.85	—
D	D1	41×41	0.62	3.70	147	5373	—
	D2	41×41	3.89	13.88	3.21	8.76	0.528
	D3	41×41	7.2	14.48	3.04	64.5	—
	D4	41×41	2.12	13.64	3.85	12.27	—

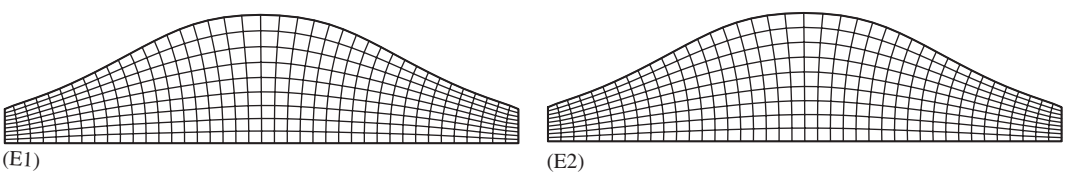

Figure 5. Meshes in domain E: (E1) RL; and (E2) improved RL with constant α in the whole domain.

Table III. Evaluation of meshes in domain E.

Domain	Case	Size	ADO	MDO	AAR	MAR	Final α
E	E1	10×41	0.30	0.82	1.60	3.14	—
	E2	10×41	0.42	0.95	1.58	3.13	0.169

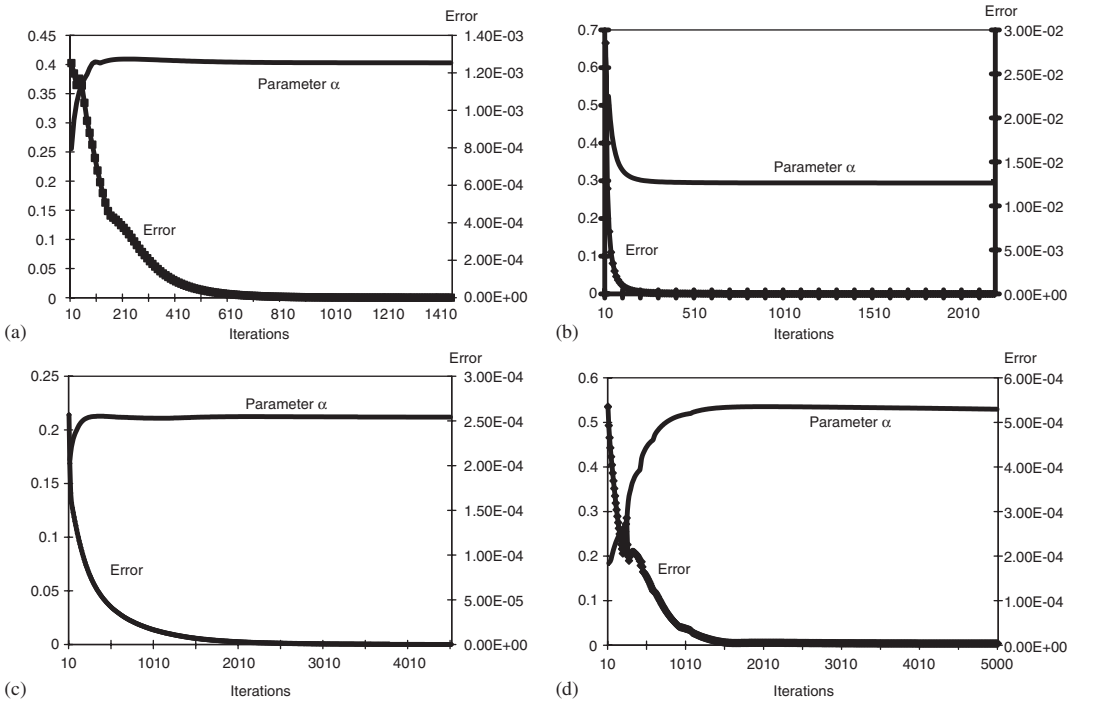

Figure 6. Convergence process: (a) domain A; (b) domain B; (c) domain C; and (d) domain D.

The initial value of the parameter α depends on the initial mesh. Then it was adjusted dynamically with the iterations and converged to a constant value. As shown in Tables I and II, the final values of α are $0.403, 0.3, 0.212$ and 0.528 for these four domains, respectively.

The final values of α for domains C and D in the present method are quite close to the parameter α used in Reference [17], in which it is constant in both space and iterations and was set to 0.2 and 0.6 for these two same domains, respectively. And the mesh qualities of these two domains using both methods are also very close. (Please refer to Reference [17] for the details of the results of these two domains.)

8. APPLICATIONS

A bay and an estuary (domains F and G) are selected to challenge the improved RL system. The layouts of these two domains are displayed in Figure 7. The boundaries of both domains

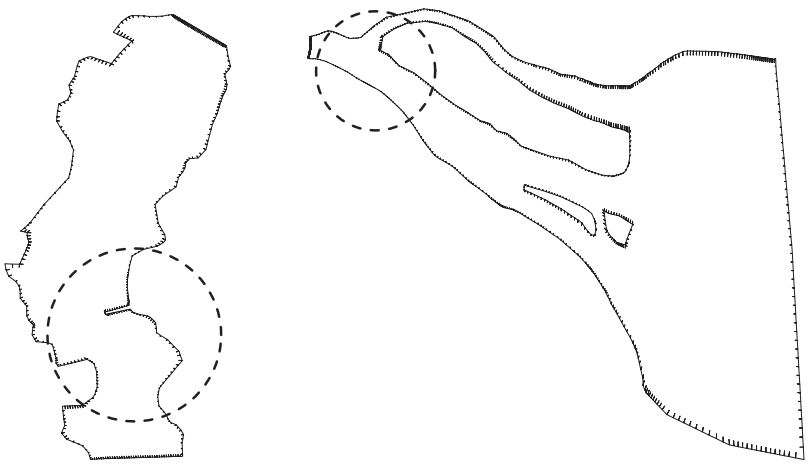

Figure 7. Layouts of Domains F and G.

are very irregular, and it is hard to apply the sliding boundary conditions. There are one spin in domain F and three islands in domain G, which made it difficult for mesh generation. The initial meshes with non-uniform nodal distribution along the boundaries were created by the algebraic method. The Dirichlet boundary conditions were used for all boundaries. In these two natural domains, the improved RL system with constant α in the whole domain is compared with the original RL system and the conformal mapping system.

Figures 8–11 show the resulting meshes and Table IV summarizes the evaluation of mesh quality. For both domains, the original RL systems failed to generate an acceptable mesh without mesh distortion and overlapping, although it produced best orthogonal meshes. As shown in Figures 9 and 11, the conformal mapping system improved the mesh smoothness greatly, but it also produced folded meshes at certain places for both domains. The best smooth mesh still comes from the improved RL with constant α in the whole domain. These two applications show that the improved RL system is quite robust and effective.

9. CONCLUSIONS

To resolve the mesh distortion and overlapping problems in geometrically complex domains when using the RL system with the 'weak constraint' method, an improved RL system with automatic smoothness control is presented in this paper. The proposed method is the further improvement of the modified RL system with contribution factors proposed by Zhang *et al.* [17], in which an empirical adjustable parameter α is used to control the strength of the contribution factors.

The improved RL system directly controls the distortion function f using the contribution factors to improve the overall mesh smoothness. Compared to the method proposed in Reference [17], the present method does not need to tune the parameter to obtain good results. Instead, an automatic smoothness control mechanism, consisting of the self-adjustment

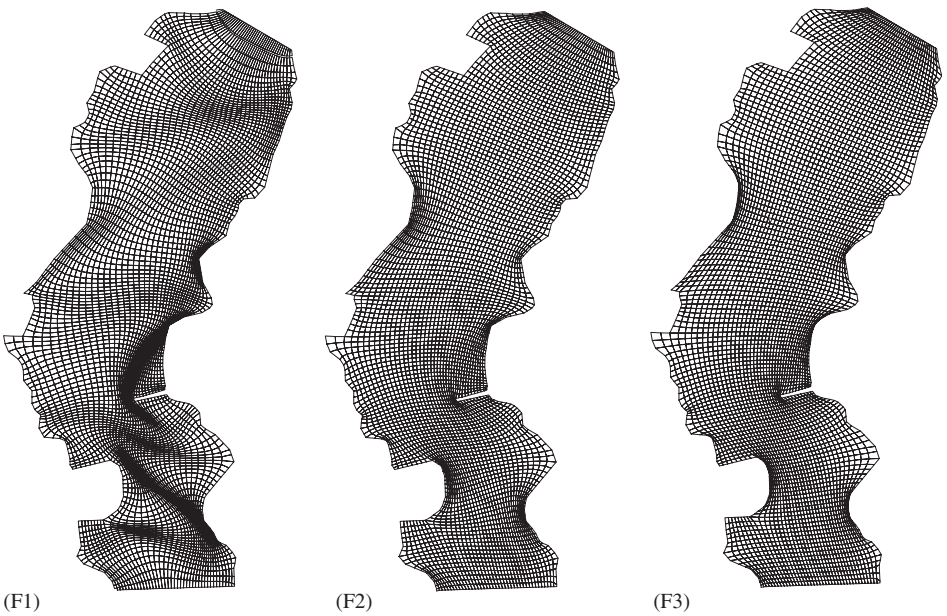

Figure 8. Meshes in domain F (global): (F1) RL; (F2) improved RL with constant α in the whole domain; and (F3) conformal mapping.

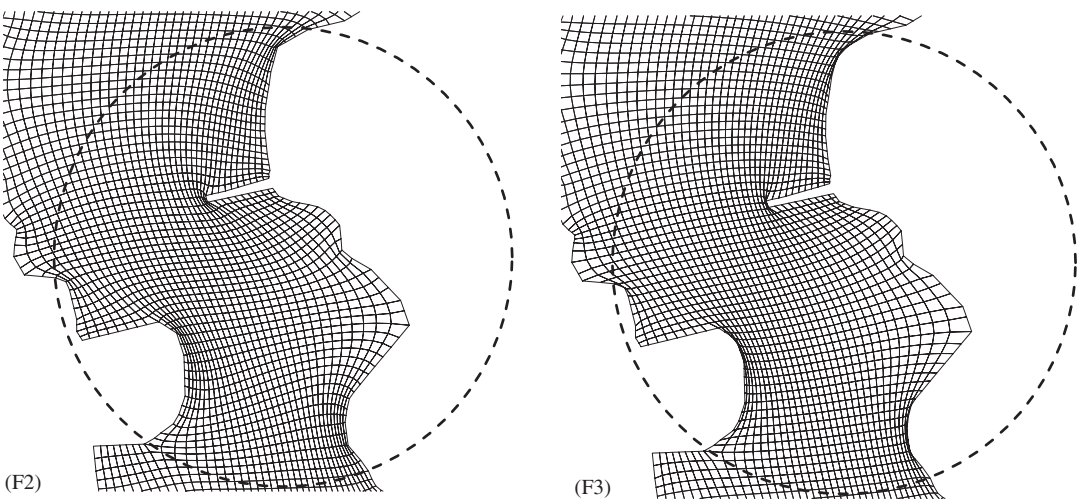

Figure 9. Meshes in domain F (local): (F2) improved RL with constant α in the whole domain; and (F3) improved RL with constant α in the whole domain.

mechanism and the auto-evaluation mechanism for α, has been established based on five types of local smoothness conditions, namely, the local relative smoothness conditions in ξ and η directions, the local absolute smoothness conditions in ξ and η directions and the local

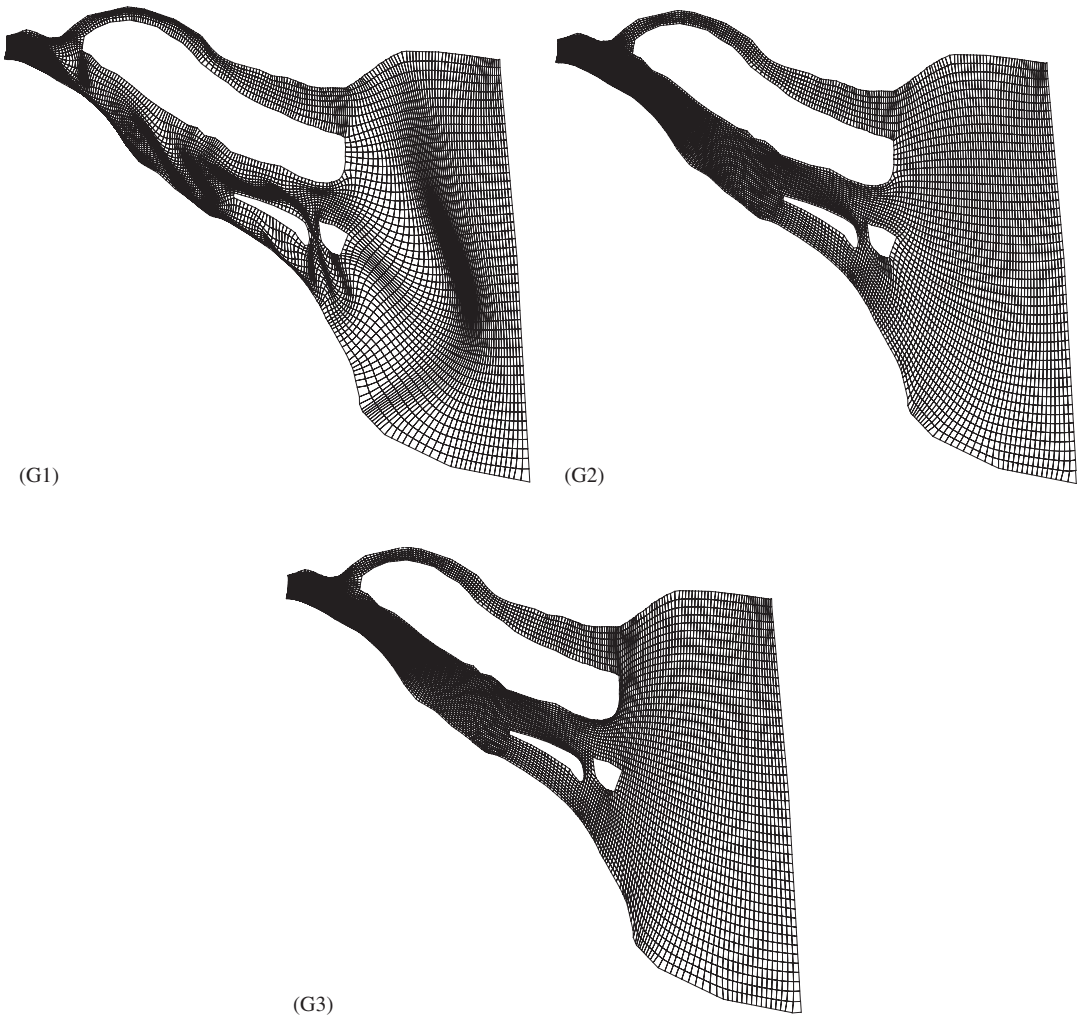

Figure 10. Meshes in domain G (global): (G1) RL; (G2) improved RL with constant α in the whole domain; and (G3) conformal mapping.

absolute smoothness conditions. An ADS is used to comprehensively characterize the local mesh smoothness. The auto-evaluation mechanism is consistent with the self-adjustment mechanism and controlled by the maximum ADS. In order to avoid the inconsistency created by the spatially varied α, the constant value of α in the whole domain is used instead. The parameter α is dynamically adjusted during the iteration process.

Although it is proposed for 2D structured mesh generation, the present method can be extended to 3D mesh generation as well. Examples and applications have shown that the proposed RL system is capable of generating nearly orthogonal meshes with a good balance of the orthogonality and the smoothness.

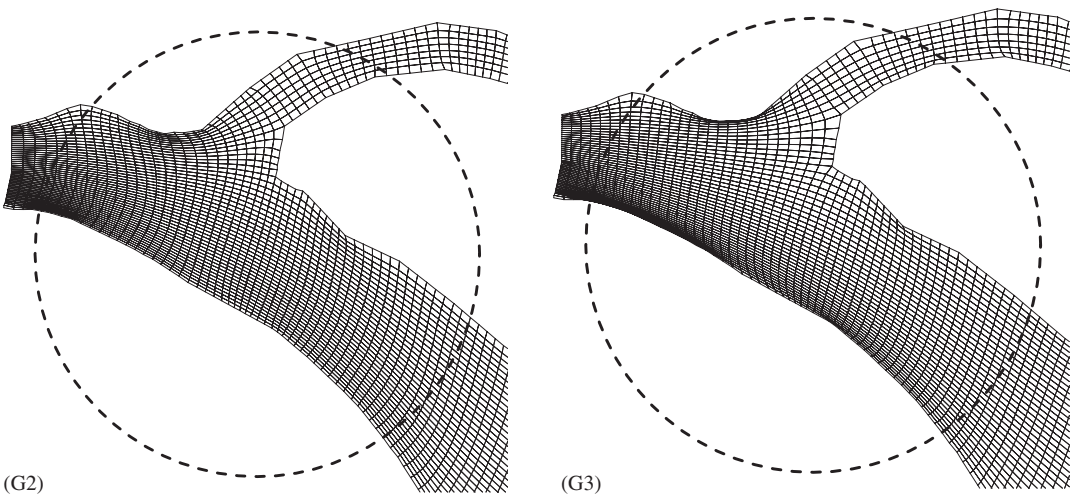

Figure 11. Meshes in domain G (local): (G2) improved RL with constant α in the whole domain; and (G3) conformal mapping.

Table IV. Evaluation of meshes in domains F and G.

Domain	Case	Size	ADO	MDO	AAR	MAR	Final α
F	F1	41×137	0.29	3.90	2.30	65.1	—
	F2	41×137	2.16	10.9	1.44	6.62	0.597
	F3	41×137	2.69	14.46	1.37	12.8	—
G	G1	49×192	0.71	8.70	27.6	1643	—
	G2	49×192	3.17	11.6	2.32	8.24	0.630
	G3	49×192	3.83	14.4	2.34	100.1	—

ACKNOWLEDGEMENTS

This work is a result of research sponsored by the USDA Agriculture Research Service under Specific Research Agreement No. 58-6408-2-0062 (monitored by the USDA-ARS National Sedimentation Laboratory) and The University of Mississippi.

REFERENCES

1. Akcelik V, Jaramaz B, Ghattas O. Nearly orthogonal two-dimensional grid generation with aspect ratio control. *Journal of Computational Physics* 2001; **171**:805–821.
2. Allievi A, Calisal SM. Application of Bubnov–Galerkin formulation to orthogonal grid generation. *Journal of Computational Physics* 1992; **98**:163–173.
3. Brackbill JU, Saltzman JS. Adaptive zoning for singular problems in two-dimensions. *Journal of Computational Physics* 1982; **46**:342.
4. Duraiswami R, Prosperetti A. Orthogonal mapping in two dimensions. *Journal of Computational Physics* 1992; **98**:254–268.
5. Eça L. 2D orthogonal grid generation with boundary point distribution control. *Journal of Computational Physics* 1996; **125**:440–453.

6. Hung TK, Brown TD. An implicit finite-difference method for solving the Navier–Stokes equations using orthogonal curvilinear coordinates. *Journal of Computational Physics* 1977; **23**:343–363.
7. Kang IS, Leal LG. Orthogonal grid generation in a 2D domain via the boundary integral technique. *Journal of Computational Physics* 1992; **102**:78–87.
8. Mobley CD, Stewart RJ. On the numerical generation of boundary-fitted orthogonal curvilinear coordinate systems. *Journal of Computational Physics* 1980; **34**:124–135.
9. Oh HJ, Kang IS. A non-iterative scheme for orthogonal grid generation with control function and specified boundary correspondence on three sides. *Journal of Computational Physics* 1994; **112**:138–148.
10. Pope SB. The calculation of turbulent recirculating flows in general orthogonal coordinates. *Journal of Computational Physics* 1978; **26**:197–217.
11. Ryskin G, Leal LG. Orthogonal mapping. *Journal of Computational Physics* 1983; **50**:71–100.
12. Tamamidis P, Assanis DN. Generation of orthogonal grids with control of spacing. *Journal of Computational Physics* 1991; **94**:437–453.
13. Thomas PD, Middlecoff JF. Direct control of the mesh node distribution in meshes generated by elliptic systems. *AIAA Journal* 1980; **18**:652–657.
14. Thompson JF, Thames FC, Mastin CW. TOMCAT—a code for numerical generation of boundary-fitted curvilinear coordinate system on fields containing any number of arbitrary two-dimensional bodies. *Journal of Computational Physics* 1977; **24**:274–302.
15. Thompson JF, Warsi ZUA, Mastin CW. *Numerical Grid Generation*: *Foundation and Application*. North-Holland: New York, 1985.
16. Thompson JF. A reflection on grid generation in the 90s: trends, needs, and influences. *5th International Conference on Grid Generation in CFS*, Mississippi State University, 1996.
17. Zhang YX, Jia YF, Wang SSY. 2D nearly orthogonal mesh generation. *International Journal for Numerical Methods in Fluids* 2004; **46**:685–707.

